Review of Scientific Instruments

Implementation of a Talbot–Lau x-ray deflectometer diagnostic platform for the OMEGA EP laser

Cite as: Rev. Sci. Instrum. **91**, 023511 (2020); https://doi.org/10.1063/1.5123919
Submitted: 09 August 2019 . Accepted: 30 January 2020 . Published Online: 19 February 2020

M. P. Valdivia, D. Stutman, C. Stoeckl, C. Mileham, J. Zou, S. Muller, K. Kaiser, C. Sorce, P. A. Keiter, J. R. Fein, M. Trantham, R. P. Drake, and S. P. Regan

View Online Export Citation CrossMark

ARTICLES YOU MAY BE INTERESTED IN

Talbot–Lau interferometry-based x-ray imaging system with retractable and rotatable gratings for nondestructive testing
Review of Scientific Instruments **91**, 023706 (2020); https://doi.org/10.1063/1.5131306

A highly precise cross-capacitive sensor for metal debris detection in insulating oil
Review of Scientific Instruments **91**, 025005 (2020); https://doi.org/10.1063/1.5139925

Design of a fast field-cycling magnetic resonance imaging system, characterization and methods for relaxation dispersion measurements around 1.5 T
Review of Scientific Instruments **91**, 024102 (2020); https://doi.org/10.1063/1.5128851

MCL MAD CITY LABS INC. www.madcitylabs.com
Nanopositioning Systems
Modular Motion Control
AFM and NSOM Instruments
Single Molecule Microscopes


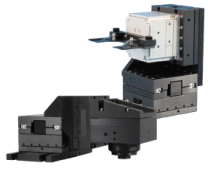
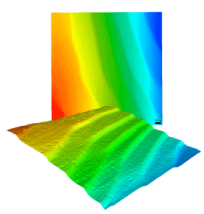
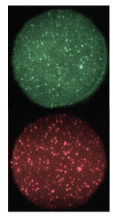

© 2020 Author(s).

Review of Scientific Instruments ARTICLE scitation.org/journal/rsi

Implementation of a Talbot–Lau x-ray deflectometer diagnostic platform for the OMEGA EP laser

Cite as: Rev. Sci. Instrum. 91, 023511 (2020); doi: 10.1063/1.5123919
Submitted: 9 August 2019 • Accepted: 30 January 2020 •
Published Online: 19 February 2020

View Online Export Citation CrossMark

M. P. Valdivia,[1,a)] D. Stutman,[1] C. Stoeckl,[2] C. Mileham,[2] J. Zou,[2] S. Muller,[3] K. Kaiser,[4] C. Sorce,[2] P. A. Keiter,[5] J. R. Fein,[6] M. Trantham,[7] R. P. Drake,[7] and S. P. Regan[2]

AFFILIATIONS

[1]Department of Physics and Astronomy, Johns Hopkins University, Baltimore, Maryland 21218, USA
[2]Laboratory for Laser Energetics, University of Rochester, Rochester, New York 14623, USA
[3]General Atomics, Inertial Fusion Technology, San Diego, California 92121, USA
[4]Microworks GmbH, 76137 Karlsruhe, Germany
[5]Los Alamos National Laboratory, Los Alamos, New Mexico 87544, USA
[6]Sandia National Laboratories, Albuquerque, New Mexico 87123, USA
[7]Climate and Space Science and Engineering, University of Michigan, Ann Arbor, Michigan 48109, USA

[a)]**Author to whom correspondence should be addressed:** mpvaldivia@pha.jhu.edu

ABSTRACT

A Talbot–Lau X-ray Deflectometer (TXD) was implemented in the OMEGA EP laser facility to characterize the evolution of an irradiated foil ablation front by mapping electron densities $>10^{22}$ cm^{-3} by means of Moiré deflectometry. The experiment used a short-pulse laser (30–100 J, 10 ps) and a foil copper target as an x-ray backlighter source. In the first experimental tests performed to benchmark the diagnostic platform, grating survival was demonstrated and x-ray backlighter laser parameters that deliver Moiré images were described. The necessary modifications to accurately probe the ablation front through TXD using the EP-TXD diagnostic platform are discussed.

Published under license by AIP Publishing. https://doi.org/10.1063/1.5123919

I. INTRODUCTION

Talbot interferometry can detect phase changes in media through beam refraction measurements.[1–3] These phase changes are induced by the electron density gradients present in an object, which is placed along a probing beam path. In the Talbot–Lau variant, the interferometer can make use of incoherent sources (such as those produced by laser–target interactions) by generating an array of quasi-coherent sources.[4–6] Moreover, fringe patterns obtained in the deflectometry mode allow for time-resolved imaging.[7,8]

In the past decade, Talbot–Lau X-ray Deflectometry (TXD) has been developed as a diagnostic for high energy density laboratory physics research.[9,10] While x-ray radiography techniques are widely used to characterize shocks,[11] materials,[12] and High Energy Density (HED) plasmas,[13] TXD uses refraction rather than attenuation to map electron density gradients, taking advantage of the higher contrast for low-Z materials when probing at 1–100 keV.[9,10] This is especially relevant when characterizing weakly absorbing plasma objects. Furthermore, it has been demonstrated that refraction-based diagnostics can enhance the visibility of features of interest in samples relevant to hydrodynamic experiments by better detecting high electron densities.[14,15] Nevertheless, current refraction diagnostics cannot detect electron densities in the high ranges that TXD can, as they are limited by the probing beam energy.[16]

Adaptations for the high-power laser environment have been implemented on the Multi-TeraWatt (MTW) and Laboratoire pour l'Utilisation des Lasers Intenses (LULI2000) laser systems.[17,18] Based on these results, a new OMEGA EP diagnostic platform was developed in order to provide electron density diagnostics $>10^{22}$ cm^{-3} to many users of the facility performing HED science research. This paper details the design of the EP-TXD diagnostic platform and its first deployment as a primary

Published under license by AIP Publishing

diagnostic to characterize the ablation front propagation of irradiated foils driven by the OMEGA EP laser.

II. TALBOT–LAU X-RAY DEFLECTOMETER: OMEGA EP DIAGNOSTIC PLATFORM

The design and implementation of any diagnostic platform in the high-intensity laser environment should consider the experiments to be characterized, laser system characteristics, vacuum chamber geometry, and the specific requirements of the diagnostic, among other factors. The first TXD diagnostic platform for the OMEGA EP laser system was setup in a standard Ten-Inch Manipulator (TIM) configuration.[19] This choice makes TXD easily adaptable to other laser systems. The interferometer was coupled to an existing TIM-based x-ray CCD imaging system (Spectral Instruments SI800), and it was deployed on the TIM14 diagnostic port after considering beam trajectories, field-of-view of other diagnostics, and location of manipulators. The Talbot–Lau interferometer has been designed to work with an 8 keV backlighter source, obtained from K-shell emission of a Cu target. One of the four OMEGA EP beams was used in short pulse mode (>100 J, 10 ps) for backlighting. The backlighter beam was chosen to backlight the interferometer in this campaign, considering foil orientation with respect to gratings as well as diagnostics and beam paths. The 8 keV backlighting capabilities are well developed for OMEGA EP[20] and were tested in previous MTW experiments.[21] The irradiated foil experiment seeks to drive a plastic foil with three long pulse beams to study the plasma ablation front evolution in the nanosecond scale.

A. Talbot–Lau interferometry

A Talbot–Lau x-ray interferometer is composed of three microperiodic gratings. A source grating (G_0), which enables coherent backlighting from the laser produced x-ray emission, a π-shift phase grating (G_1), which acts as a beam-splitter, and an analyzer grating (G_2), which converts the refraction-induced phase into intensity changes.[22,23] The gratings are aligned by orienting all grating bars parallel to each other. To enable Moiré deflectometry, the phase grating is rotated by a small angle. The specific details and schematics of Talbot–Lau x-ray deflectometry for high-power laser environments can be found in Refs. 10, 17, 18, 24–27.

A Talbot–Lau interferometer detects electron density (n_e) gradients according to the following equation for refraction angle α:

$$\alpha(y) = \frac{1}{n_c}\int_{-\infty}^{\infty}\frac{\partial n_e(x,y)}{\partial y}\mathrm{dx}. \quad (1)$$

In TXD, Moiré fringe shift measurements are directly proportional to the phase change. In turn, the phase change determines the angular refraction produced by the electron density gradients in the probed object. The EP-TXD diagnostic platform has an angular sensitivity[10] (refraction angle equivalent to one fringe shift) of W_{eff} = 150 ± 3 μrad for G_0 to a backlighter target distance of 2 mm and W_{eff} = 180 ± 3 μrad for G_0 to backlighter target distance of 5 mm. It has been demonstrated that at least 10% to a few fringe shifts can be measured with the TXD technique.[18]

As discussed in Ref. 10, the refraction angle is given by the phase change ($\Delta\Phi$) and the wavelength (λ) as follows:

$$\alpha(x,y) = \lambda/2\pi\Delta\Phi(x,y). \quad (2)$$

In the deflectometry configuration, one fringe shift is equivalent to the system effective angular sensitivity. From Eq. (1), considering a critical density of $n_c = 4.56 \times 10^{28}$ cm^{-3} at 8 keV, the OMEGA EP Talbot–Lau x-ray deflectometer platform is optimized to measure an electron density of ~10^{23-24} cm^{-3}.

B. Irradiated foils experiment

1. Motivation

A detailed understanding of electron transport and ablation in laser-produced plasmas requires accurate knowledge of plasma density and temperature profiles near and below critical density. Considerable experimental, theoretical, and simulation work has been done to understand electron density profiles in laser-produced plasmas.[28] Discrepancies between simulation and experimental results at high intensities are not yet fully understood. Imaging diagnostics have measured irradiated foil ablation fronts but are limited to densities <10^{21} cm^{-3}. Therefore, these diagnostics are not able to image the critical density region, where heat flux is strongest[16] and nonlocal electron transport becomes significant at laser intensities near and above 10^{15} W/cm^2.

Density measurements in laser-produced plasmas are well suited for a first test of the TXD diagnostic platform because of the experimental simplicity and the modeling challenge they represent. An experiment to study the plasma ablation dynamics of 3 mm × 3 mm × 120 μm CH foil targets irradiated at ~10^{15} W/cm^2 was recently reported in the literature.[29] The electron density can be probed through TXD and compared to previous results obtained with the transmission and scattering of light at the laser frequency, the scattering of light at 3/2 of the laser frequency, the spectrum of Raman-scattered light, the x-ray spectrum from doped targets, and the image of the ultraviolet bremsstrahlung emission from the plasma.[30,31] These measurements are generally not consistent with two-dimensional computer simulations.

2. Implementation

Plastic (CH) foils were irradiated with three long pulse OMEGA EP beams. Each 1 ns pulse at maximum energy per beam (~2 kJ) with wEP-SG8-0750 phase plates delivers a total laser irradiance >8×10^{14} W/cm^2. Since the irradiated foil weakly attenuates x-ray energies near 8 keV, it behaves as a phase object where the x-ray interaction is dominated by refraction. The expected refraction angles in these laser-produced plasmas are in the ~50–150 μrad range. To achieve angular sensitivity in the range described above, the distance between G_0 and the target was maximized.[32] Separation between the backlighter beam and driver lasers was limited to ~1.8 cm due to beam pointing restrictions. The short G_0 to target distance possible at OMEGA EP requires a small period source grating for sufficient angular sensitivity. A source grating of 2.4 μm period was placed 5 mm or 2 mm from the backlighter target, while the CH foil target was placed 13 mm or 16 mm from the source

Published under license by AIP Publishing

grating. Thus, the effective angular width of the interferometer was ~120 μrad.[10]

The experimental plan consisted of up to eight laser shots. The first half of shots were used to measure the angular and spatial resolution. These shots did not require the main laser beams, and only the backlighter beam was used to irradiate a 1.8 mm × 0.8 mm × 20 μm Cu foil to obtain 8 keV radiation. A static test object, either a tantalum foil (200 μm × 500 μm × 1.8 mm) or a nylon rod of 100 μm radius and 1.8 mm length, was imaged. This image can determine the density gradient dynamic range given by the x-ray source and aid in the electron density retrieval by providing a reference image. Due to the short distance between the source and the backlighter target, the grating is expected to be destroyed after each shot. Nevertheless, Moiré fringe formation prior to grating disintegration is expected. To that aim, the backlighter target to G_0 distances of 5 mm and 2 mm were probed.

Once Moiré fringe formation was demonstrated, the long pulse beams irradiated the CH foil target of 3 mm × 3 mm × 120 μm to study ablation dynamics (Fig. 1). The open-drive geometry of the CH target allowed radiographic access to the ablation profile. To probe the ablation front from 0.5 ns to 1.5 ns, backlighter beam timing was kept constant, while timing of long pulse beams was modified.

Moiré images were recorded with a direct detection x-ray CCD with quantum efficiency >50% at 8 keV. The efficiency decreases rapidly at higher energies, thus making the detector mostly "blind" to the high energy photons created by relativistic electrons in the backlighter foil.[31] The hard x-ray self-emission from the laser-illuminated CH target was expected to be negligible, and thus, it was operated in time integrated mode. Thin foils (15 μm Al or 25 μm Cu) were used to filter lower energy emission. Additionally, image plates were considered as an alternative detector. Image plates have been shown to work at ~10 keV in high energy density plasma (HEDP) experiments,[33,34] although their sensitivity to higher energy x-rays is higher than that of the x-ray CCD. A photon budget of at least a few 100 photons per pixel was calculated assuming ~7×10^{-4} conversion efficiency of laser light to Cu K-α photons,[35,36] considering 20% interferometer transmission at 8 keV, and an attenuation factor of 6 in the blast shield, detector light blocking filter, and the CH target. The plasma induced Moiré fringe shifts are measured with respect to the reference pattern. Thus, electron density mapping follows the standard procedure for the TXD technique.[20]

The plasma and backlighter targets were remotely positioned in between G_0 and G_1 and behind G_0, respectively. Both were staged using separate target positioners to allow greater freedom for distance adjustments, in particular, to vary the backlighter target to G_0 distance. The backlighter target was irradiated at 45° and the focal spot was adjusted for a peak incident intensity of $<10^{19}$ W/cm^2 in order to achieve efficient conversion of laser light into Cu K-α photons, while minimizing the production of high energy bremsstrahlung photons. A 10 ps laser pulse was used to ensure that the source grating will survive long enough to produce a Moiré image that can be used in electron density retrieval.

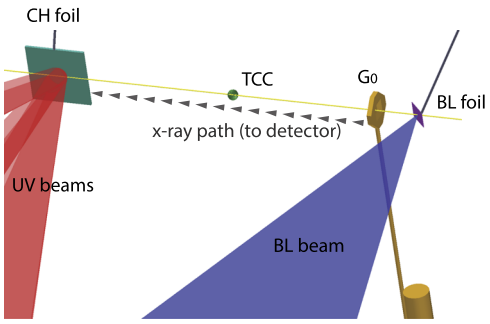

FIG. 1. VisRad schematic of the irradiated foils experiment. Backlighter (BL) foil to G_0 distance of 2 mm or 5 mm and G_0 to CH foil distance of 16 mm or 13 mm, respectively.

3. Simulations

To assess the performance of the TXD method, simulations of the OMEGA EP irradiated foil experiment were performed. A 2D CRASH[37] simulation is shown in Fig. 2, where a CH foil target is irradiated using 351 nm lasers (6500 J total energy) with a spot radius of 358 μm.

Figure 3 shows synthetic Moiré deflectometry images generated with X-ray waveFront propagation (XWFP)[38] software. The 2D density profiles shown in Fig. 6(a) cannot be simulated with XWFP, which is limited to spherical and cylindrical objects. Hence, the data were analyzed as follows: First, 1D electron density profiles perpendicular to the foil were extracted from the 2D CRASH simulation at 200 ps [Fig. 6(a)] for three different radii. Then, the profiles were used to simulate rods of variable density (along the axial direction). These simulations provided a general idea of the fringe shift to be observed in the deflectometer images.

Simulations show discernible fringe shifts in the regions of higher electron density gradients, as expected. Moreover, the deflectometry images show regions of extreme electron density gradients, evidenced as a loss of fringe contrast. Nevertheless, these simulations demonstrate that the EP-TXD diagnostic can deliver measurable Moiré fringe shifts in the irradiated foil experiment.

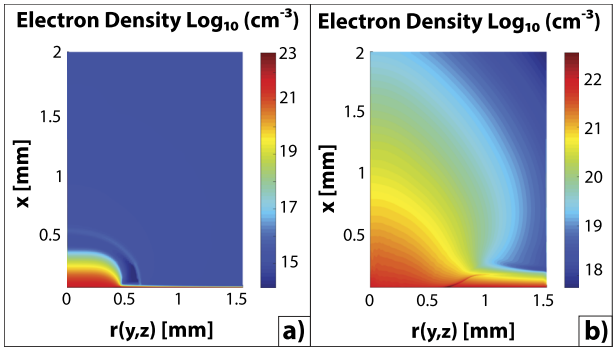

FIG. 2. 2D CRASH of the plasma produced by hitting a CH foil with three OMEGA EP long pulse beams. Radial profiles at (a) 200 ps and (b) 1.5 ns are shown. X direction corresponds to the axis perpendicular to the foil plane and r(y,z) corresponds to the foil plane, following the axes definition in Fig. 1.

Published under license by AIP Publishing

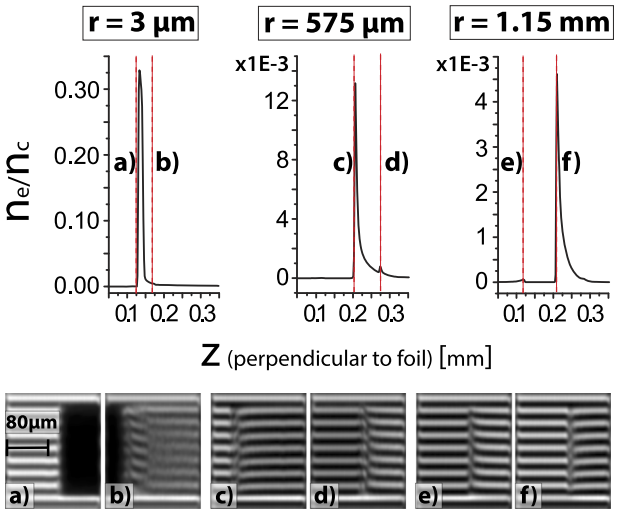

FIG. 3. Top: normalized 1D electron density profiles for three different radii (tracked perpendicular to the foil, along the ablation front expansion) extracted from 2D CRASH simulation [Fig. 6(a)] of a CH foil of 3 mm^2 × 120 μm. Bottom: Moiré deflectograms were simulated for the extracted 1D ablating profiles shown above, probed at 8 keV for two locations (shown in red) perpendicular to the foil. For radial distances of r = 3 μm, (a) shows the highest density peak and (b) shows a moderate electron density value. For r = 575 μm, (c) shows the highest density peak in the region selected and (d) shows a smaller secondary electron density peak. For r = 1.15 mm, (e) shows a small electron density peak, while (f) shows the highest density peak in the area simulated.

C. EP-TXD diagnostic platform

1. TXD rail

Based on vacuum chamber dimensions and diagnostic port locations, the interferometer was set in the m = 7 Talbot order and ~5.2 Talbot magnification so that the distance between the phase grating and the plasma object could be maximized while keeping the total interferometer length under 100 cm (Fig. 3). In this configuration, the nominal G_0 to G_1 gratings distance was 109.0 mm and 554.0 mm between G_1 and G_2 gratings. The system object magnification is ~41 to 45, therefore obtaining the source size limited spatial resolution considering detector pixels of 13.5 μm. In Talbot–Lau interferometry, the spatial resolution is limited by the source size similar to radiographic systems. If the backlighter source size greatly exceeds the source grating period, then the spatial resolution is improved through a "micro-source effect." Nevertheless, this is not expected in the current configuration. With a 26 × 26 mm^2 detector area, the field of view at the target was ~0.8 × 0.8 mm^2, adequate for the proposed plasma target. A Cu light-tight filter (25 μm or 50 μm thick) was placed in front of the X-ray CCD detector.

TABLE I. Range of motion and resolution of G_1 and G_2 adjustments.

	Z (mm)	θ_X (°)	θ_Y (°)	θ_z (°)
G_1 range of motion	±17	±5	±5	±10
G_1 resolution	0.004	0.004	0.004	0.17
G_2 range of motion	±25	±4	±4	±10
G_2 resolution	0.004	0.003	0.003	0.17

The EP-TXD design (Fig. 4) enabled G_1 and G_2 to move translationally and rotationally. The G_1 and G_2 gratings were mounted on stainless steel rings, which could be rotated in their housings and locked in position. The rotational stages were mounted on translational stages which enabled inter-grating distance changes. The range of motion and resolution of the adjustments for G_1 and G_2 are summarized in Table I.

Moiré fringe patterns were obtained through a small rotation between G_1 and G_2 gratings.[10,39] In order to obtain a specific period and fringe orientation, the gratings must be aligned precisely. Any rotational or translational misalignment will decrease the Moiré fringe contrast. Thus, all gratings were mounted on a common optical rail to ensure stable and accurate alignment of the Talbot–Lau x-ray deflectometer. The rail was installed inside a TIM manipulator and operated as the front-end of an x-ray CCD.

The phase grating was protected by a blast shield (15 μm Al or 25 μm Cu) and expected to survive each shot, while the source

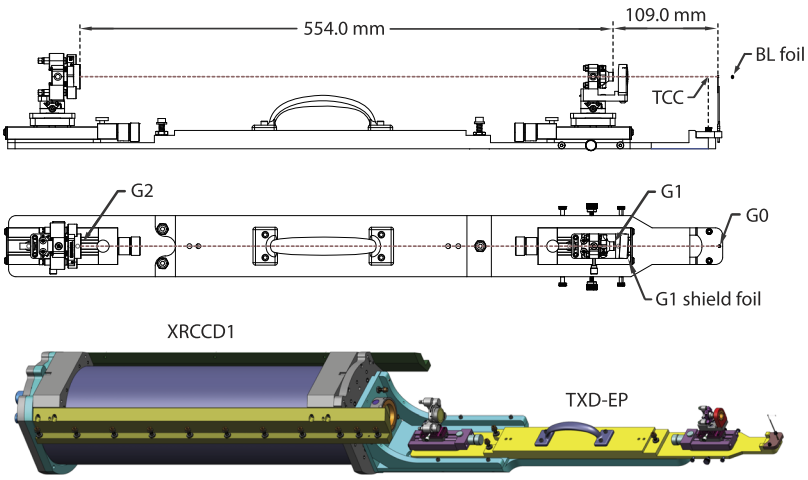

FIG. 4. EP-TXD diagnostic platform. Top: rail design including inter-grating distances. Bottom: EP-TXD rail as the front-end of XRCCD1 TIM diagnostic.

Published under license by AIP Publishing

grating had to be replaced after each laser shot. G_0 rotation was fixed, and thus, the analyzer and phase gratings were independently aligned with respect to it. Rotational and translational adjustments were made until the maximum fringe contrast was obtained (25%–28%). Filter transmission curves and interferometer contrast curves (simulated with XWFP) for the diagnostic platform are shown in Fig. 5 below. Moreover, critical electron density is determined by the wavelength of the probing beam, and thus, the accuracy of electron density measurements determined through TXD depends on the spectral bandwidth, as shown in Eq. (2).

The alignment of TXD rails was performed onsite outside the OMEGA EP chamber and TIM boat. X-ray alignment used a Cu anode x-ray tube emitting x rays at 8 keV and an x-ray CCD (Andor Ikon-M) of similar characteristics to the one used in the experiment. A reference Moiré pattern was recorded after the alignment of each rail. The reference image was used to obtain phase information needed in the electron density gradient mapping process.[27] Additionally, these images also provided fringe contrast and period reference values.

2. Source grating modifications

Similar to previous adaptations,[20] G_1 and G_2 were supported by a 10 μm thin polyimide membrane. The fabrication process is routinely used by Microworks[40] to make masks for x-ray lithography.[41] The analyzer grating used gold as the absorber pattern with a height of ~15 μm. The phase grating used nickel as the phase shift material with a height of 3.0 μm.

G_0 fabrication and mounting presented challenges when designing the interferometer adaptation for OMEGA EP. Due to backlighter beam proximity, the first diffraction grating G_0 is expected to be destroyed after each shot, and hence, the grating should be considered when accounting for total debris produced per shot, along with plasma and backlighter foils. Therefore, the total mass of G_0 was substantially reduced from previous TXD systems.[20]

New gratings were designed and manufactured to meet the OMEGA EP adaptation requirements. The outer dimensions of the frame were reduced from 5 × 5 mm^2 to 1.8 × 1.8 mm^2. The effective area (inner window size) was reduced from 6.25 mm^2 to 0.25 mm^2 (0.5 × 0.5 mm^2). While the mass of the gratings used in previous experiments was above 10 mg, the mass of the new gratings was reduced to approximately 1 mg. These changes imposed grating design and manufacturing limitations. The gratings used previously were manufactured on a 2.5 μm thick titanium membrane and then released from the processing wafer and glued on commercially available silicon frames.[42] In contrast, the new gratings were made of gold lamellae within a polymer matrix and stayed on the wafer. The frame was created by anisotropic wet etching of the silicon 100 wafer from the back side, while a 40 nm thin chromium layer was used for processing. The result was a self-supporting grating without an additional membrane. The new source grating is shown in Fig. 6 below.

It was found that the source grating surface contained macrostructures that alter the Moiré pattern,[18,27] During preliminary x-ray alignment, a correlation was made between the depth of the macrostructures and severity of the fringe alteration. Hence, source gratings were visually inspected prior to mounting to select the gratings with shallowest deformations, as these seemed to result in less alteration of the fringe pattern.

Final assembly of the G_0 mount was done on-site at the Laboratory for Laser Energetics (LLE). A standard OMEGA stalk was

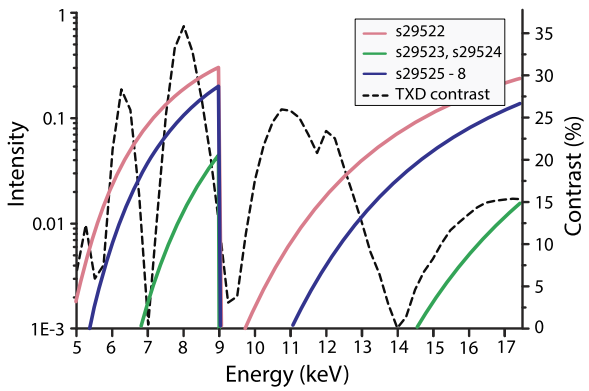

FIG. 5. Filter transmission curves for the first shot (G_0 = 20 μm Cu, G_1 = 15 μm Al, and G_2 = 12.5 μm Cu), second and third shots (G_0 = 20 μm Cu, G_1 = 25 μm Cu, and G_2 = 50 μm Cu), and fourth to seventh shots (G_0 = 20 μm Cu, G_1 = 15 μm Al, and G_2 = 25 μm Cu). Interferometer contrast curve for the m = 7 Talbot order used in the irradiated foil experiment is shown as well.

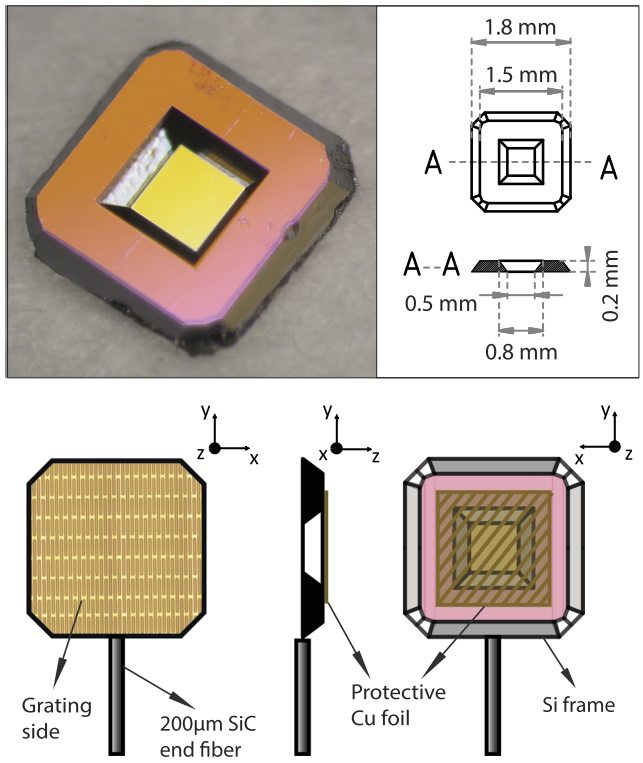

FIG. 6. Source grating image and schematics. The diffraction grating gold membrane was supported by a Si octagon frame designed to minimize the total grating mass. Views are shown for a mounted G_0 package: from grating side (including a microscope image of the grating at ~40:1 scale), edge-on, and backlighter side. Coordinate axes are defined for reference to critical rotation alignment tolerances.

Published under license by AIP Publishing

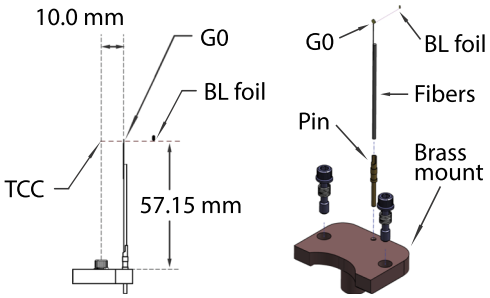

FIG. 7. G_0 mount configuration. Left: schematic of the fiber and stalk installed on the removable brass mount. Right: individual G_0 mount parts. The brass mount piece attaches to TXD rail platform.

constructed to hold each G_0 package at the required height along the rail axis with ±1.0 mm accuracy, as shown in Fig. 7. The stalk consisted of a connector pin at the base, followed by a carbon fiber rod and a 200 μm diameter SiC end fiber. This provided a rigid support for the G_0 package with minimal added mass.

The G_0 gratings were mounted to the stalk assemblies with ±1.0° rotation accuracy about the x- and z-axes, as defined in Fig. 1, so that grating bars were aligned normal to the rail base, in order to properly probe the plasma ablation front. The alignment was done under a camera-equipped microscope with the assistance of measurement software, 3-axis micromanipulators, and a simple vacuum fixture to hold the Si G_0 frame in place. Following the stalk mounting process, a protective Cu foil of 20 μm thickness was glued to the Si frame on the backlighter side to protect the grating from ablation due to laser heating during the experiment. Each stalk-mounted G_0 assembly was installed in a removable brass mount via the connector pin, as shown in Fig. 2. The brass mount allowed for efficacious replacement of the source grating after each shot and allowed for easy alignment of the phase and analyzer gratings relative to the fixed source grating. The stalk to brass mount alignment was also done under a microscope using a custom fixture designed to mate to the brass base in the same fashion and with the same tolerances as the source end of the rail system. Once the G_0 mount was installed, any additional error in vertical alignment was within the rotation and translation capabilities of the rail design.

III. RESULTS

A. Moiré fringe formation

A backlighter beam of 28.4 J, 10 ps, and 50 μm FWHM spot size yielded ~665 photons per pixel with a backlighter to source grating distance of 5 mm and 75 μm Cu filtration (3% transmission at 8 keV). A Moiré fringe contrast of <1% was measured. Hard hits on the x-ray CCD were measured at a level of >3000 counts, with a ~1.1 signal-to-noise ratio. A second Moiré image was obtained with a backlighter beam of 48.7 J, 10 ps, and 70 μm spot size. A photon count of ~1000 was obtained with lower filtration (26% transmission at 8 keV) for a backlighter foil to source grating distance of 2 mm. A fringe contrast of ~12% to 15% was measured, compared to the 26%–28% obtained with a Cu x-ray tube. Hard hits reached a level of <21 000 counts, with ~1.8 signal-to-noise ratio.

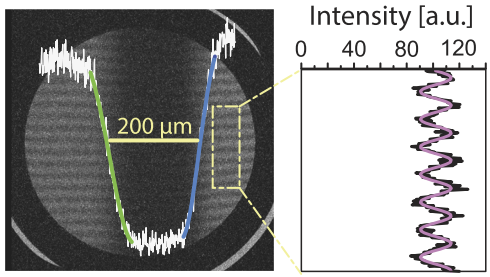

FIG. 8. Moiré image of a Ta test object (200 μm × 1.75 mm × 1.5 mm) recorded with the x-ray CCD. Moiré fringe contrast plot shown on the right.

B. Backlighter and detector performance

Figure 8 shows a Moiré image of a resolution target placed 16 mm away from the source grating (as shown in Fig. 5). In this shot, the backlighter laser beam was used to image a Ta slab of 200 μm × 1.75 mm × 0.5 mm instead of a laser-driven CH foil. Through the edge method, a FWHM of 60.3 ± 2.0 μm was measured.

Due to x-ray CCD electronics failure, no additional Moiré images could be obtained with the CCD detector. To continue the experiment, image plates (Fuji SR) were implemented directly in front of the x-ray CCD filter plane. The following shots aimed at image irradiated foil ablation profiles through TXD, as originally planned, now using a new detector system. Nevertheless, no discernible Moiré fringes were recorded with the image plates.

C. Electron density measurements

Following the results shown in Fig. 8, the CH foil was irradiated with three UV beams at maximum energy with a backlighter beam pulse of 48.7 J, 10 ps and 70 μm spot size. As mentioned previously, no image was obtained due to electromagnetic pulses, which caused an error in CCD electronics readout. This rendered the detector unavailable for the remaining laser shots. The x-ray CCD was replaced with image plates; however, no Moiré images were recorded from an irradiated foil ablation front, and thus, electron density mapping of a plasma object was not achieved.

IV. DISCUSSION

The first backlighter laser shot performed at best focus ($I \sim 10^{18}$ W/cm^2) saturated the detector. Filtering was increased for the following shot, reducing 8 keV emission to <10% and >30 keV to 50%. Nevertheless, this x-ray CCD image was saturated as well. Previous results at MTW,[20] with intensities of 2.7×10^{15} W/cm^2 to 2.7×10^{16} W/cm^2, delivered photon counts at the detector well below saturation (~1% of maximum counts). Considering source to detector distances and filtering, ~50% of maximum counts were expected. Hence, the increased x-ray production observed can be attributed to a higher conversion efficiency for backlighters generated with laser intensities >10^{17} W/cm^2.[43–45]

Recognizing the above, laser intensity for subsequent backlighter shots is decreased by defocusing the laser spot size. Experiments studying x-ray backlighters in the 17–75 keV energy range have defocused the laser spot size to reduce bremsstrahlung

Published under license by AIP Publishing

background by increasing the laser intensity while optimizing the K_α yield.[46] Moiré fringes were recorded with the x-ray CCD camera for laser pulses of 53.8 μm spot size and 28.4 J energy (Fig. 8). Nevertheless, low photon count was observed, with a signal-to-noise ratio of <1.2, which can be attributed to the high x-ray filtering setup used on the previous shot.

For the following shot, x-ray filtering was reduced in order to optimize photon flux, particularly for 8 keV emission. Further defocusing to 61.9 μm was implemented, delivering a similar laser intensity of ~1.6×10^{17} W/cm^2. This setup yielded higher Moiré contrast and better signal-to-noise (SNR). Filtering modification from 50 μm Cu to 15 μm Al increases 8 keV signal to >40x and an increase close to 10x for energies >30 keV. While this second Moiré image showed an improved SNR, it was lower than that expected from filter modification. This is attributed to an increase in bremsstrahlung radiation and hard x-ray coronal emission, which can offset the K_α emission signal.

The first goal toward establishing TXD as a standard HED plasma diagnostic was achieved. Moiré deflectometry images were recorded. Since the angular resolution is optimized by increasing the object to source grating distance (Fig. 3), it follows that the backlighter target to source grating distance must be reduced to achieve better angular sensitivity. It was demonstrated that a 2.4 μm period source grating, 2 mm away from a backlighter target, can survive a <50 J, 10 ps laser pulse long enough to provide electron density gradient information. Due to laser pointing limitations, the maximum distance between the backlighter laser and driver beams is ~1.8 mm. It should be noted that smaller distances would facilitate diagnosis of experiments where refraction angles <100 μrads are expected. Particularly, better angular sensitivity could map electron densities closer to quarter critical, which can be useful when comparing electron density measurements from previous angular filter refractometry and hydrodynamic simulations.[29] This would bring forth new information on hot electron production in studies of laser-irradiated planar foils related to stimulated Raman scattering and two-plasmon decay.

An x-ray backlighter source size of 60.3 ± 2.0 μm was determined. While other studies have measured source sizes 5–10x larger than the laser spot size due to the spreading of the relativistic electrons,[47] the source size obtained from Moiré images is consistent with the smaller "effective" source size expected in Talbot–Lau interferometry due to the effect of the source grating period.[10,48] Moreover, this measurement is in agreement with XWFP simulations. In future, the improved spatial resolution should be investigated by exploring alternative backlighter target configurations, which will also benefit Moiré fringe contrast as smaller sources emit brighter K_α radiation.[47] While wire backlighters have demonstrated improved resolution,[49] these are prone to EMPs, as observed in previous experiments. Alternatively, a similar scheme illuminating the backlighter target in and edge-on geometry has shown improved spatial resolution.[46,47]

For laser-driven CH foil shots, improved quality images (Moiré contrast, photon count, SNR, etc.) were attained by further increasing the laser energy. Saturation of x-ray CCD (>32 000 counts) was observed for an intensity of ~5×10^{17} W/cm^2. In comparison, x-ray backlighter laser intensities five times lower delivered close to 1000 counts at the detector. The much higher photon count at the detector (even when taking into account emission from the probed plasma object) indicates that conversion efficiency should be carefully investigated to achieve adequate K_α emission with high SNR and Moiré contrast closer to that obtained with a medical x-ray tube (>20%).

As mentioned previously, image plates replaced the CCD detector once its electronics failed. No Moiré fringes were observed for plasma shots. A subsequent shot lowered x-ray backlighter laser energy to 47.7 J to reproduce the intensity parameters used in the best Moiré image recorded with a x-ray CCD camera (1.6×10^{17} W/cm^2). Similar to the previous shot, no Moiré fringes were observed. It should be noted that in both images, the stainless-steel and aluminum grating rotation stages were recorded. The absence of fringes and the presence of higher Z components are understood in context with detector response between the x-ray CCD and image plates. Specifically, the x-ray CCD gain is ~50% for 8 keV, 25% for 10 keV, 5% for 20 keV, and >1% for 30 keV, favoring emission detection at <10 keV. In comparison, SR image plates have a gain of ~100% for 10 keV, >80% for 20 keV, and ~40% for 30 keV. Moreover, the gain increases to >50% for 40 keV.[34] Considering that laser-produced backlighters emit monoenergetic line radiation in addition to a smooth bremsstrahlung background,[50] low Moiré fringe contrast can be understood by considering the interferometer contrast curve (Fig. 4).

Furthermore, image plates are typically used to record higher x-ray energies, which should be considered when analyzing the results obtained. Experiments requiring monochromatic K_α sources to diagnose the areal mass density have used both the x-ray film and image plates.[51] For x-ray film, the signal to background ratio was found to be ~1, while image plates data produced higher background. Given that x-ray CCD detectors have been demonstrated to yield better Moiré fringe contrast when compared to x-ray film,[17] it follows that Moiré fringe contrast measured from the EP-TXD diagnostic platform is expected to be much lower for image plates, which corroborates the results obtained. Furthermore, LULI experiments recorded Moiré fringes using image plates with a much lower contrast than that expected from x-ray CCD measurements (9% compared with ~30%). Conversely, no fringes were observed in the presence of a plasma target.[17] This reinforces the notion that Moiré contrast using image plates is effectively extinguished due to emission outside the optimal energy band for Cu K_α.

V. SUMMARY

A Talbot–Lau x-ray deflectometer has been implemented for the OMEGA EP laser. The EP-TXD diagnostic platform was tested and experimental results determined the parameters at which Moiré images can be obtained. These results will establish a base line for future experiments that will seek to map electron density gradients in HEDP experiments through Talbot–Lau interferometry. The limitations and requirements for a TIM-based TXD diagnostic platform have been established. Specifically, the specific changes necessary to optimize the quality of Moiré images and diagnose irradiated foil ablation fronts through TXD have been identified. First, x-ray backlighter performance must be optimized. The source size must be reduced to achieve the high spatial resolution needed to characterize the ablation front evolution. It should be noted that Moiré fringe contrast will also benefit from the improved spatial resolution by enhancing the TXD phase retrieval process. Similarly, x-ray

Published under license by AIP Publishing

emission spectra must be narrowed down to optimize fringe contrast considering the interferometer contrast curve. While energies lower than 8 keV can be filtered easily, it is not the case for higher energies. This requires careful consideration of hot electron production effects on the relative intensity of Cu K_α line emission and bremsstrahlung background emission.

Changes in the laser focal spot size can decrease the intensity while optimizing the ratio of line and broadband emission; however, this requires careful consideration of laser parameters as well as backlighter target geometry. Moreover, detector performance must be compared, considering gain in and outside the sought-after energy range. The x-ray CCD camera, image plates, and x-ray film should be investigated. To improve the spatial resolution, future studies should investigate bookend wires[52] in addition to wire and foil backlighters in an end-on geometry. Additionally, TXD should be modified to operate in monochromatic mode using a multilayer mirror that can select radiation emission in the optimal energy band. This is expected to maximize interferometer contrast and enable the use of image plates, which would be an operational advantage since they are not susceptible to system EMPs. It is expected that once the TXD diagnostic platform for the OMEGA EP laser is optimized, it will enable plasma electron density mapping at 10^{23} cm^{-3} and above, thus bringing new information to the HEDP field.

ACKNOWLEDGMENTS

We would like to thank the Laboratory for Laser Energetics Engineering and scientific staff for their support in the implementation of the EP-TXD diagnostic platform and their efforts over the years in the development and improvement of the TXD diagnostic technique. Their help and constant support have been an invaluable asset to our team. This work was supported by U.S. DoE/NNSA (Grant Nos. DE-NA0002955 and DE-NA0003526), with work at Michigan supported by DE-NA0002956.

REFERENCES

[1] H. F. Talbot, "LXXVI. Facts relating to optical science. No. IV," London, Edinburgh Dublin Philos. Mag. J. Sci. **9**, 401–407 (1836).
[2] D. E. Silva, "Talbot interferometer for radial and lateral derivatives," Appl. Opt. **11**, 2613–2624 (1972).
[3] A. Momose *et al.*, "Demonstration of x-ray Talbot interferometry," Jpn. J. Appl. Phys., Part 2 **42**, L866–L868 (2003).
[4] M. Engelhardt *et al.*, "The fractional Talbot effect in differential x-ray phase-contrast imaging for extended and polychromatic x-ray sources," J. Microsc. **232**, 145–157 (2008).
[5] W. B. Case, M. Tomandl, S. Deachapunya, and M. Arndt, "Realization of optical carpets in the Talbot and Talbot-Lau configurations," Opt. Express **17**, 020966 (2009).
[6] L. Liu, "Partially coherent diffraction effect between Lau and Talbot effects," J. Opt. Soc. Am. A **5**, 1709–1716 (1988).
[7] N. Bevins, J. Zambelli, K. Li, Z. Qi, and G.-H. Chen, "Multicontrast x-ray computed tomography imaging using Talbot-Lau interferometry without phase stepping," Med. Phys. **39**, 424 (2012).
[8] H. Guo, "Phase-shifting deflectometric Moiré topography," Structural Longevity **5**, 39–47 (2011).
[9] D. Stutman and M. Finkenthal, "Talbot-Lau x-ray interferometry for high energy density plasma diagnostic," Rev. Sci. Instrum. **82**, 113508 (2011).
[10] M. P. Valdivia, D. Stutman, and M. Finkenthal, "Talbot-Lau based Moiré deflectometry with non-coherent sources as potential High Energy Density plasma diagnostic," J. Appl. Phys. **114**, 163302 (2013).
[11] G. W. Collins *et al.*, "Measurements of the equation of state of deuterium at the fluid insulator – metal transition," Science **281**, 1178–1182 (1998).
[12] T. J. Davis, D. Gao, T. E. Gureyev, A. W. Stevenson, and S. W. Wilkins, "Phase-contrast imaging of weakly absorbing materials using hard X-rays," Nature **373**, 595–598 (1995).
[13] T. A. Shelkovenko, D. B. Sinars, S. A. Pikuz, and D. A. Hammer, "Radiographic and spectroscopic studies of X-pinch plasma implosion dynamics and x-ray burst emission characteristics," Phys. Plasmas **8**, 1305 (2001).
[14] J. A. Koch *et al.*, "Refraction-enhanced x-ray radiography for inertial confinement fusion and laser-produced plasma applications," J. Appl. Phys. **105**, 113112 (2009).
[15] Y. Ping *et al.*, "Refraction-enhanced x-ray radiography for density profile measurements at CH/Be interface," J. Instrum. **6**, P09004 (2011).
[16] D. Haberberger, S. Ivancic, S. X. Hu, R. Boni, M. Barczys, R. S. Craxton, and D. H. Froula, "Measurements of electron density profiles using an angular filter refractometer," Phys. Plasmas **21**, 056304 (2014).
[17] M. P. Valdivia *et al.*, "X-ray backlighter requirements for refraction-based electron density diagnostics through Talbot-Lau deflectometry," Rev. Sci. Instrum. **89**, 10G127 (2018).
[18] M. P. Valdivia, D. Stutman, and M. Finkenthal, "Moire deflectometry using the Talbot-Lau interferometer as refraction diagnostic for High Energy Density plasmas at energies below 10 keV," Rev. Sci. Instrum. **85**, 073702 (2014).
[19] LLE. National, Laser Users Facility Users Guide.
[20] M. P. Valdivia *et al.*, "An x-ray backlit Talbot-Lau deflectometer for high-energy-density electron density diagnostics," Rev. Sci. Instrum. **87**, 023505 (2016).
[21] M. P. Valdivia *et al.*, "Talbot-Lau x-ray deflectometer electron density diagnostic for laser and pulsed power high energy density plasma experiments (invited)," Rev. Sci. Instrum. **87**, 11D501 (2016).
[22] F. Pfeiffer, T. Weitkamp, O. Bunk, and C. David, "Phase retrieval and differential phase-contrast imaging with low-brilliance X-ray sources," Nat. Phys. **2**, 258–261 (2006).
[23] A. Momose, W. Yashiro, Y. Takeda, Y. Suzuki, and T. Hattori, "Phase tomography by X-ray talbot interferometry for biological imaging," Jpn. J. Appl. Phys., Part 1 **45**, 5254–5262 (2006).
[24] M. P. Valdivia *et al.*, "A Talbot – Lau X-ray deflectometer as a high-energy density plasma diagnostic," IEEE Trans. Plasma Sci. **44**, 1592–1598 (2016).
[25] D. Stutman, M. P. Valdivia, and M. Finkenthal, "X-ray Moiré deflectometry using synthetic reference images," Appl. Opt. **54**, 5956–5961 (2015).
[26] M. Valdivia, D. Stutman, and M. Finkenthal, "Talbot-Lau x-ray density diagnostic for High Energy Density plasmas," in *2015 IEEE 26th Symposium on Fusion Engineering (SOFE)* (IEEE, 2015), pp. 1–5.
[27] M. P. Valdivia *et al.*, "Talbot – Lau x-ray deflectometry phase-retrieval methods for electron density diagnostics in high-energy density experiments," Appl. Opt. **57**, 13–15 (2018).
[28] L. Da Silva *et al.*, "Electron density measurements of high density plasmas using Soft X-ray laser interferometry," Phys. Rev. Lett. **74**, 3991–3994 (1995).
[29] J. R. Fein *et al.*, "Mitigation of hot electrons from laser-plasma instabilities in high-Z, highly ionized plasmas," Phys. Plasmas **24**, 032707 (2017).
[30] R. P. Drake *et al.*, "Hydrodynamic expansion of exploding-foil targets irradiated by 0.53 μm laser light," Phys. Fluids B **1**, 1089 (1989).
[31] A. Ravasio *et al.*, "Hard x-ray radiography for density measurement in shock compressed matter," Phys. Plasmas **15**, 3–6 (2008).
[32] A. Momose, W. Yashiro, and Y. Takeda, "Sensitivity of x-ray phase imaging based on Talbot interferometry," Jpn. J. Appl. Phys. **47**(10), 8077 (2008).
[33] N. Izumi *et al.*, "Application of imaging plates to x-ray imaging and spectroscopy in laser plasma experiments (invited)," Rev. Sci. Instrum. **77**, 10E325 (2006).
[34] B. R. Maddox *et al.*, "High-energy x-ray backlighter spectrum measurements using calibrated image plates," Rev. Sci. Instrum. **82**, 023111 (2011).
[35] P. M. Nilson *et al.*, "Scaling hot-electron generation to long-pulse, high-intensity lasersolid interactions," Phys. Plasmas **18**, 056703 (2011).
[36] P. M. Nilson *et al.*, "Time-resolved Ka spectroscopy measurements of hot-electron equilibration dynamics in thin-foil solid targets: Collisional and collective effects," J. Phys. B: At., Mol. Opt. Phys. **48**, 224001 (2015).

Published under license by AIP Publishing

[37]B. Van Der Holst *et al.*, "Crash: A block-adaptive-mesh code for radiative shock hydrodynamics – implementation and verification," Astrophys. J. Suppl. Ser. **194**, 23 (2011).
[38]T. Weitkamp, "XWFP: An x-ray wavefront propagation software package for the IDL computer language," Adv. Comput. Methods X-Ray Neutron Opt. **5536**, 181–189 (2004).
[39]J. Jahns and A. W. Lohmann, "The Lau effect (a diffraction experiment with incoherent illumination)," Opt. Commun. **28**, 263–267 (1979).
[40]See https://www.micro-works.de for Microworks. Microworks GmbH.
[41]S. Achenbach, Æ. M. Boerner, and Æ. S. Kinuta, "Structure quality in deep X-ray lithography applying commercial polyimide-based masks," Microsyst. Technol. **13**, 349–353 (2007).
[42]M. Gad-el-Hak, *MEMS: Applications* (CRC Press, 2005).
[43]P. M. Nilson *et al.*, "Scaling hot-electron generation to high-power, Kilojoule-class laser-solid interactions," Phys. Rev. Lett. **105**, 235001 (2010).
[44]P. M. Nilson *et al.*, "High-intensity laser-plasma interactions in the refluxing limit," Phys. Plasmas **15**, 056308 (2008).
[45]J. Myatt *et al.*, "High-intensity laser interactions with mass- limited solid targets and implications for fast-ignition experiments on OMEGA EP," Phys. Plasmas **14**, 056301 (2007).
[46]H. S. Park *et al.*, "High-resolution 17–75 keV backlighters for high energy density experiments," Phys. Plasmas **15**, 072705 (2008).
[47]H.-S. Park *et al.*, "High-energy Kα radiography using high-intensity, short-pulse lasers," Phys. Plasmas **13**, 056309 (2006).
[48]F. Gori, "Lau effect and coherence theory," Opt. Commun. **31**, 4–8 (1979).
[49]A. Casner, C. Mailliet, A. Rigon, S. F. Khan, and D. Martinez, "From ICF to laboratory astrophysics: Ablative and classical Rayleigh–Taylor instability experiments in turbulent-like regimes," Nucl. Fusion **59**, 032002 (2018).
[50]P. Neumayer *et al.*, "The role of hot electron refluxing in laser-generated K -alpha sources," Phys. Plasmas **17**, 6–12 (2010).
[51]C. M. Krauland *et al.*, "An evaluation of high energy bremsstrahlung background in point-projection x-ray radiography experiments," Rev. Sci. Instrum. **83**, 1–4 (2012).
[52]W. Theobald *et al.*, "High-intensity laser-plasma interaction with wedge-shaped-cavity targets," Phys. Plasmas **17**, 1–7 (2010).

Published under license by AIP Publishing